Microfluidic Platform for Combinatorial Synthesis and Optimization of Targeted Nanoparticles for Cancer Therapy

Pedro M. Valencia,[†] Eric M. Pridgen,[†] Minsoung Rhee,[‡,§] Robert Langer,[†,⊥,*] Omid C. Farokhzad,[‡,⊥,*] and Rohit Karnik[§,*]

[†]Department of Chemical Engineering, Massachusetts Institute of Technology, Cambridge, Massachusetts 02139, United States, [‡]Laboratory of Nanomedicine and Biomaterials and Department of Anesthesiology, Brigham and Women's Hospital, Harvard Medical School, Boston, Massachusetts 02115, United States, [§]Department of Mechanical Engineering, Massachusetts Institute of Technology, Cambridge, Massachusetts 02139, United States, and [⊥]MIT-Harvard Center for Cancer Nanotechnology Excellence, Massachusetts Institute of Technology, Cambridge, Massachusetts 02139, United States

ABSTRACT Taking a nanoparticle (NP) from discovery to clinical translation has been slow compared to small molecules, in part by the lack of systems that enable their precise engineering and rapid optimization. In this work we have developed a microfluidic platform for the rapid, combinatorial synthesis and optimization of NPs. The system takes in a number of NP precursors from which a library of NPs with varying size, surface charge, target ligand density, and drug load is produced in a reproducible manner. We rapidly synthesized 45 different formulations of poly(lactic-*co*-glycolic acid)-*b*-poly(ethylene glycol) NPs of different size and surface composition and screened and ranked the NPs for their ability to evade macrophage uptake *in vitro*. Comparison of the results to pharmacokinetic studies *in vivo* in mice revealed a correlation between *in vitro* screen and *in vivo* behavior. Next, we selected NP synthesis parameters that resulted in longer blood half-life and used the microfluidic platform to synthesize targeted NPs with varying targeting ligand density (using a model targeting ligand against cancer cells). We screened NPs *in vitro* against prostate cancer cells as well as macrophages, identifying one formulation that exhibited high uptake by cancer cells yet similar macrophage uptake compared to nontargeted NPs. *In vivo*, the selected targeted NPs showed a 3.5-fold increase in tumor accumulation in mice compared to nontargeted NPs. The developed microfluidic platform in this work represents a tool that could potentially accelerate the discovery and clinical translation of NPs.

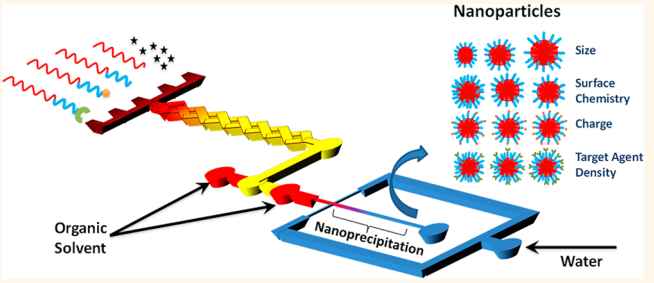

KEYWORDS: microfluidics · nanoparticle · nanomedicine · rapid synthesis · mixing

Nanoparticles (NPs) able to encapsulate and deliver thousands of drug molecules per particle hold tremendous potential for treating various diseases such as cancer, inflammation, and infectious diseases.[1] Despite the high level of activity and enthusiasm focused on the development of NP therapeutics over the past 30 years, very few NP formulations have reached clinical translation and human impact.[2] In fact, while there are myriads of proof-of-concept studies presenting novel NPs that target and kill cancer cells, there are significantly fewer examples where the engineering and optimization is carried out to reach clinical translation. In part, the challenge lies in the complexity of NP optimization, since for every disease type it is necessary to find the optimal interplay of biophysicochemical parameters (size, charge, surface composition, *etc.*) that simultaneously confers molecular targeting, immune evasion, and controlled drug release.[3,4] In addition, technology platforms for the rapid synthesis of NPs with a wide range of properties in a reproducible manner are only now starting to emerge.[5−7]

Microfluidics, the science and technology of manipulating nanoliter volumes in microscale fluidic channels, has impacted a range of applications including biological analysis, chemical synthesis, single cell analysis, and

* Address correspondence to ofarokhzad@zeus.bwh.harvard.edu; karnik@mit.edu; rlanger@mit.edu.

Received for review July 2, 2013 and accepted November 4, 2013.

Published online 10.1021/nn403370e

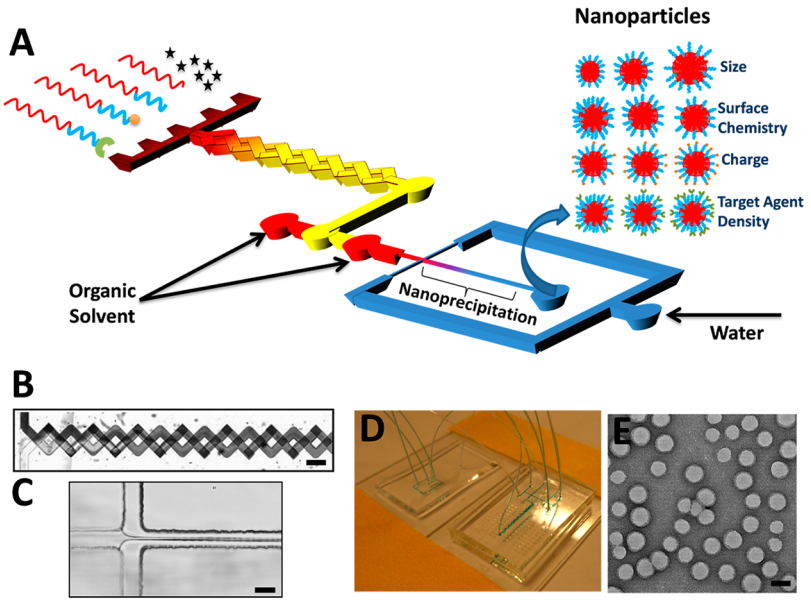

Figure 1. Microfluidic platform for rapid synthesis of NPs. (A) Schematic of system where NP precursors enter a multi-inlet mixer at different ratios producing a library of NPs upon self-assembly. (B) Mixer in operation showing complete mixing of streams at the end of the mixer. Scale bar = 200 μm. (C) Image of hydrodynamic flow-focusing where NPs self-assemble through nanoprecipitation. Scale bar = 20 μm. (D) Photograph of microfluidic devices for mixing of NP precursors and NP synthesis. (E) Image of representative NPs produced by the system. Scale bar = 50 nm.

tissue engineering.[8] In nanomedicine, microfluidics has enabled the synthesis of NPs with narrower size distributions, improved batch-to-batch reproducibility, and higher drug loadings.[9,10] Some key advantages of microfluidics include simplicity and reproducibility of device fabrication and potentially lower cost of materials due to the ability to handle small volumes. These advantages make the use of microfluidics ideal for the development of a platform that enables rapid synthesis and optimization of NPs.[11]

In the present work, inspired by the rapid, combinatorial synthesis of small molecules[12,13] and novel biomaterials,[14] we have developed a microfluidic platform for the rapid, combinatorial synthesis of NPs. Previously, we developed a microfluidic device that used 3D hydrodynamic focusing to create NPs of different sizes, in a reproducible manner, using four different polymeric precursors.[15] However, the device did not have the capability to mix precursors prior to nanoprecipitation and was not amenable to high-throughput screening. Here, we developed a fully integrated microfluidic device with a multi-inlet micromixer[16] to allow for programmable and systematic mixing of a large number of precursors before nanoprecipitation occurs. As a proof of concept, we demonstrate that this system allows for the synthesis of NPs with a wide range of properties, with batch-to-batch reproducibility, by combining over 15 different NP precursors in different ratios. For each formulation, we produced merely tens of micrograms of NPs, enough for rapid *in vitro* evaluation. Next, we show the rapid NP evaluation capabilities of the platform by synthesizing 45 different formulations with different sizes and surface compositions, screening them for macrophage uptake *in vitro*, and comparing the results with *in vivo* pharmacokinetic studies. Finally, we use the microfluidic system to synthesize targeted and nontargeted NPs with the same size and charge, and compare their tumor accumulation *in vivo*. These studies have broad implications in nanomedicine, where such a platform could be used to rapidly optimize promising novel lipid and polymeric NPs and move them quickly to preclinical studies.

RESULTS

Microfluidic Platform for Rapid Development of NPs. The microfluidic platform is composed of a multi-inlet mixing unit and a synthesis unit that operate in continuous flow mode (Figure 1A). In the mixing unit, a number of NP precursors dissolved in organic solvent are introduced in different inlets and mixed at various ratios in a 3D micromixer[16] (Figure 1B). In the synthesis unit, each precursor combination is rapidly mixed with water using a technique called 3D hydrodynamic flow focusing, where the NP precursors are squeezed three-dimensionally to a thin stream that rapidly diffuses with water, resulting in self-assembly of NPs through the process of nanoprecipitation[15] (Figure 1C). Each mixing unit inlet is connected to a syringe driven by a programmable syringe pump, which allows for precise control over the ratio of precursors that ultimately defines the physicochemical properties of the resulting NP. The flow rates of the input NP precursors can be altered periodically, resulting in sequential synthesis of a library of NPs with distinct properties and compositions. A photograph of the device is presented in

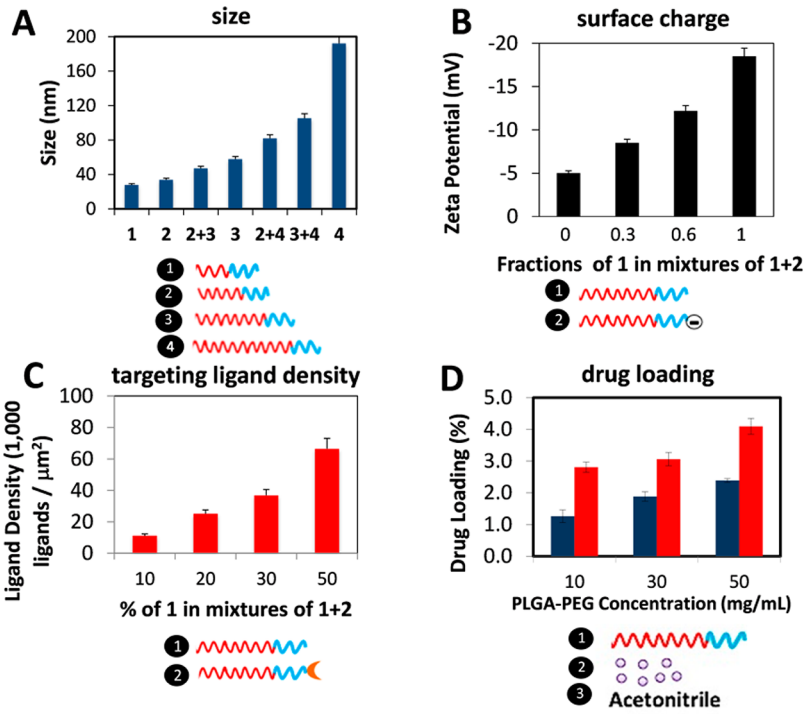

Figure 2. Synthesis of PLGA-PEG NPs with control over physicochemical properties. (A) Variation of NP size by mixing polymers with different PLGA MWs. 1, $PLGA_{10K}$-PEG_{5K}; 2, $PLGA_{27K}$-PEG_{5K}; 3, $PLGA_{45K}$-PEG_{5K}; 4, $PLGA_{95K}$-PEG_{5K}. (B) Variation of NP surface charge by mixing polymers with different end functional group on the PEG block. The carboxyl group (−COOH) is negatively charged, while methoxy group ($-OCH_3$) is neutral. 1, $PLGA_{45K}$-PEG_{5K}-OCH_3; 2, $PLGA_{45K}$-PEG_{5K}-COOH. (C) Variation of targeting ligand density by mixing polymers functionalized with targeting ligand (PLGA-PEG-LIG) together with unmodified polymer. 1, $PLGA_{27K}$-PEG_{5K}; 2, $PLGA_{45K}$-PEG_{5K}-LIG. (D). Variation of drug loading by mixing a polymer at a high concentration (50 mg/mL) with different ratios of drug (to vary initial drug loading) and plain acetonitrile (to vary concentration). 1, $PLGA_{27K}$-PEG_{5K}; 2, docetaxel; 3, acetonitrile. Blue bar, initial drug loading of 5%; red bar, initial drug loading of 10%. Legend: blue block = PEG; red block = PLGA. Error bars denote ± SD.

Figure 1D, and a TEM micrograph of representative NPs obtained with this system is shown in Figure 1E. To synthesize a diverse library of NPs, we used 15 different precursors based on poly(lactic-*co*-glycolic) acid-*b*-polyethylene glycol (PLGA-PEG) (Table S1). These included PLGA-PEG with different end functional groups to control surface charge (*e.g.*, amine, carboxyl, methoxy), PLGA MWs to control NP size (10, 27, 45, and 95 kDa), and PEG MWs to control hydrophilicity (2, 5, and 10 kDa); PLGA-PEG functionalized with *S*,*S*-2-[3-[5-amino-1-carboxypentyl]ureido]pentanedioic acid, a small-molecule ligand (LIG) that targets prostate-specific membrane antigen (PSMA) receptors overexpressed in prostate cancer cells;[17,18] and PLGA with different fluorescent probes for NP detection.

Tuning of NP Properties by Mixing Precursors in Distinct Ratios. To demonstrate the versatility of the platform, we synthesized a number of NPs spanning a wide range of physicochemical properties by strategically varying the ratios of different NP precursors. For instance, to vary the NP size we mixed PLGA-PEG with different PLGA MWs ranging from 10 to 95 kDa, resulting in sizes ranging from 25 nm up to 200 nm (Figure 2A). For varying surface charge, previous studies reported that NPs composed of PLGA-PEG-NH_2 exhibited a zeta potential of +10 to 15 mV, while NPs composed of PLGA-PEG-COOH exhibited a zeta potential of −10 to −15 mV, and those composed of PLGA-PEG-OCH_3 remained neutral.[19,20] Therefore, by mixing polymer solutions containing, for instance, OCH_3 and COOH, it was possible to tune the surface charge from neutral to highly negative (Figure 2B). For varying surface ligand density, we mixed PLGA-PEG-LIG with unmodified PLGA-PEG at different ratios, resulting in estimated ligand densities on the order of 10^3−10^5 ligands/μm^2 (*i.e.*, ~10^1−10^3 ligands per NP) (Figure 2C).[21] Finally, for varying the final drug loading of the NPs, using docetaxel as model drug, we varied both the initial drug loading and the polymer concentration in acetonitrile—factors that were previously shown to affect drug loading.[22,23] In this case, one stream contained the drug, another contained PLGA-PEG of a specific MW at 50 mg/mL, and plain acetonitrile was in a third stream to modify the concentration from 50 mg/mL down to 10 mg/mL (Figure 2D). Finally, these NPs were prepared with excellent batch-to-batch reproducibility and much narrower size distributions compared to conventional bulk synthesis (Figure S2). These results show that it is possible to reproducibly create a library of NPs spanning a broad range of NP properties by combinatorially mixing a small number of NP precursors, mostly derived from PLGA-PEG-based polymers.

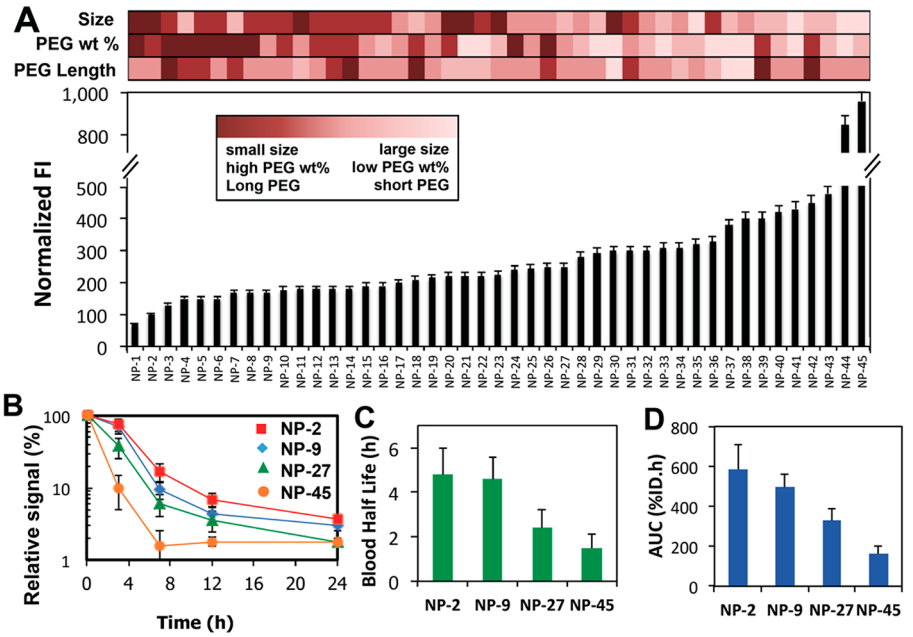

Figure 3. Synthesis and screening of 45 NPs with different sizes and PEG coverage. (A) Fluorescence intensity (FI) of macrophages associated with Alexa-488-labeled NPs. Heat map indicating extent of size, PEG weight %, and average PEG length for each formulation. (B) Pharmacokinetic profile measured by the relative fluorescence of Alexa-647-labeled NPs in blood. (C) Circulation half-life and (D) area under the curve of selected formulations with increasing macrophage binding and uptake. See Table S2 for details of the NP formulations. Error bars denote ± SD.

Rapid Development and Screening of NP Library. Next, to show the utility of our system for rapid synthesis and screening of NPs, we selected seven polymers containing different PLGA and PEG MWs mentioned above as well as free PLGA (45 kDa) to synthesize a library of NPs comprising 45 distinct formulations with different sizes and PEG coverage (see Table S2). We focused on identifying optimal nontargeted NPs by varying three key parameters known to affect *in vivo* NP behavior:[24,25] (1) NP size, (2) PEG coverage, and (3) PEG molecular weight. While NP charge is known to also affect the blood circulation half-life, we chose PEG with neutral terminal groups based on our previous studies reporting that charged NPs tend to induce complement activation more readily than neutral NPs.[20,26] For the screening, we used an established *in vitro* macrophage binding and uptake assay,[21] in which the extent of interaction between macrophages and NPs depends on the NP physicochemical properties. In this assay, fluorescently labeled NPs were incubated with macrophages in 96-well plates and then analyzed with flow cytometry using a high-throughput robotic sampler. Depending on the particle dosing per well and number of repeats per formulation, the time to synthesize 45 formulations may take from minutes to hours. In the present case, the synthesis of 45 NP formulations that were dosed at 100 μg of NPs per well at $n = 3$ required approximately 70 min, whereas by conventional pipetting it could take up to 10 times longer[7] and would likely be less reproducible.

Figure 3A shows the fluorescence intensity associated with NP binding and uptake by macrophages for the 45 formulations. For each formulation, we also measured NP size, estimated the PEG weight % from the input flow rates, and reported the average PEG length (Table S2). The results indicate that NP formulations of small size (25−30 nm), relatively high PEG wt % (up to 33%), and longer PEG molecules (up to 10 kDa) are taken up least by macrophages, which agrees with previous results reported on PEG-functionalized NPs.[24,27] Interestingly, it was observed that NP size was a key determinant in macrophage association more so than PEG coverage. For instance, a 30 nm NP with a PEG length of 5 kDa was taken up less than a 50 nm NP with a 10 kDa length. These results not only provided insight into the behavior of NPs exposed to macrophages but also demonstrated that coupling rapid microfluidic NP synthesis with conventional high-throughput screening methods enabled a large number of NPs to be evaluated in a relatively short amount of time.

In vivo, NPs tend to be taken up by the mononuclear phagocytic system mostly in the liver and the spleen, which directly affects their circulation time.[28] Consequently, it would be expected that NP uptake by macrophages *in vitro* serves as a first indication of the NP pharmacokinetics (PK) *in vivo*. To evaluate this hypothesis, we selected four representative formulations showing different macrophage uptake behaviors ranging from minimal to maximal, and investigated their PK profile *in vivo*. For this experiment, we increased the scale of production 2 orders of magnitude from hundreds of micrograms to tens of milligrams by simply programming the microfluidic system to run for a longer period of time (~50 min per formulation).

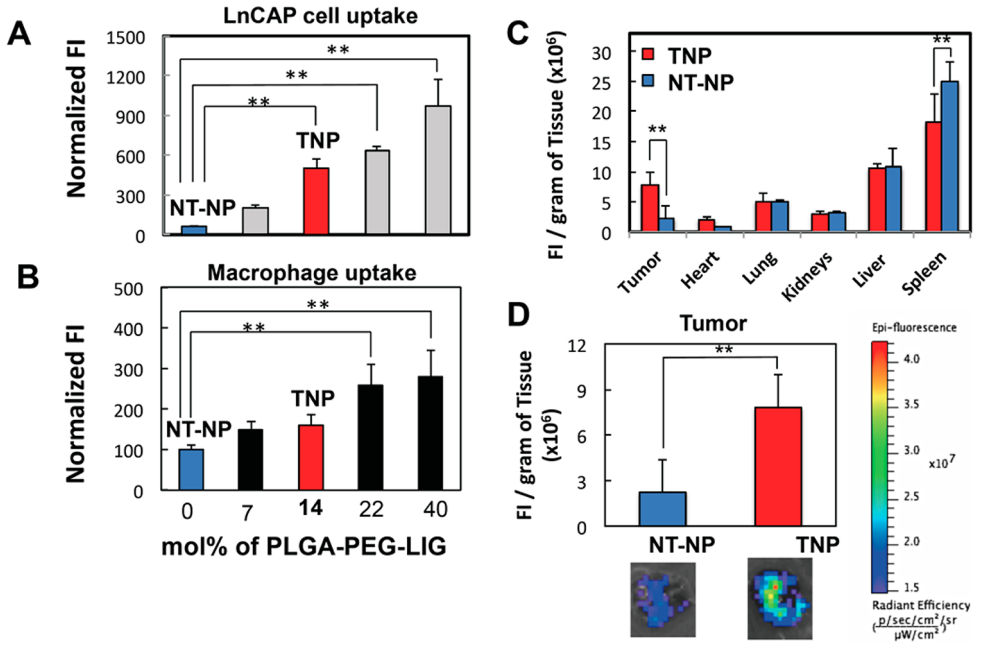

Figure 4. Comparison of biodistribution and tumor accumulation of targeted and nontargeted NPs with similar biophysicochemical properties. (A and B) Fluorescence intensity of Alexa-488-labeled targeted NPs associated with LNCaP cells (A) and macrophages (B) normalized by that of nontargeted NPs. Blue and red bars indicate nontargeted and targeted NP formulations, respectively, selected for *in vivo* studies. (C) Biodistribution and (D) tumor accumulation of a targeted NP composed of 14 mol % PLGA-PEG-LIG and nontargeted NP. **Statistically significant by *t* test with $p < 0.005$. Error bars denote ± SD.

Interestingly, the NP properties remained essentially identical across batches of different scales, which we consider a key advantage of the system. Figure 3B shows the PK profile of selected NP formulations that exhibited increasing macrophage uptake. Analysis of the PK profile revealed that the NP formulation with the lowest macrophage uptake had the longest half-life (Figure 3C) and greatest area under the curve (which is the integral of the concentration over time, expressed as % of initial dose × time) (Figure 3D). These results confirm the hypothesis that NPs with higher macrophage interactions tend to circulate in blood for a shorter amount of time.[29−31]

Screening of NPs with Different Targeting Ligand Densities. In addition to NP physicochemical properties including size, surface charge, and PEG coverage, targeting ligands can be used in an attempt to preferentially accumulate NPs in target tissues.[26] On this basis, we used the microfluidic system to synthesize targeted NPs with different targeting ligand densities, with the goal of finding one with maximum targeting ligand-mediated specific uptake with minimum macrophage uptake. Similar to previous experiments, the model targeting ligand used was LIG, which targets PSMA receptors overexpressed on LNCaP cells (a model prostate cancer cell line).[17,18] We started with the parameters identified in the previous screen that minimized macrophage uptake, *i.e.*, low NP size and high PEG coverage both obtained by using $PLGA_{27K}$-PEG_{5K} as initial precursor in formulation NP-2. We added increasing amounts of $PLGA_{45K}$-PEG_{5K}-LIG to the combination of precursors used for synthesis of NP-2 to rapidly synthesize targeted NPs (TNPs) with different ligand densities, followed by screening them *in vitro* against LNCaP cells as well as macrophages. Figure 4A and B show the cancer cell and macrophage uptake, respectively, for five different formulations containing increasing amounts of ligands on the NP surface. The results indicated that when adding up to 14 mol % of PLGA-PEG-LIG with respect to total PLGA-PEG plus PLGA-PEG-LIG to the NP formulation, a significant increase in uptake by cancer cells was observed with only a small difference in macrophage uptake compared to nontargeted NPs (NT-NPs). Beyond 14 mol % PLGA-PEG-LIG, a significant increase in macrophage uptake was observed. Interestingly, TNPs with up to 14 mol % of PLGA-PEG-LIG exhibited essentially the same average size and charge as those with unmodified PLGA-PEG (40 nm and −0.5 mV) (Figure S2), thus providing an attractive model to compare the tumor accumulation of TNPs *versus* NT-NPs.

Next, we used TNP with 14 mol % formulation (corresponding to approximately 200 ligands per NP) and performed *in vivo* studies to compare their biodistribution and tumor accumulation with NT-NPs. For the *in vivo* studies, we implanted 1×10^7 LNCaP cells in the flank of the mouse and let the tumor grow for 3−4 weeks to a size of approximately 400−600 mm^3. TNPs and NT-NPs labeled with Alexa Fluor 647 were injected *via* tail vein. After 24 h the animals were sacrificed and

the fluorescence in the organs was measured (Figure 4C). While the fluorescence signal in most of the organs was similar for both formulations, two main differences were observed for the spleen and tumor, where TNP showed significantly higher accumulation in tumor and less in the spleen *versus* the NT-NPs. In fact, the signal accumulation of TNPs in the tumor was close to 3.5-fold that of the NT-NP (Figure 4D).

DISCUSSION

While we report here the synthesis of PLGA-PEG NPs, any polymer and polymer−ligand conjugate that undergo self-assembly by nanoprecipitation[26] in water could potentially be synthesized using the microfluidic platform, and any drug that preferably interacts with the polymer *versus* water could be encapsulated. However, the organic solvent used must be compatible with the polymer, ligand, drug, and polydimethylsiloxane (PDMS) used for device fabrication.

The microfluidic platform allows for synthesis of more homogeneous, tunable NPs.[11,15,33] Three key determinants of the NP size and polydispersity are (1) the polymer properties (*e.g.*, chemical structure, molecular weight), (2) degree of interaction of polymer with organic solvent, and (3) the mixing time of organic solution and water during nanoprecipitation.[33] While there are a number of ways to control NP size, our results indicate that by simply mixing polymers having different MWs of the hydrophobic block at different ratios, one can have tighter control over a wide range of NP sizes. When mixing two polymers with different PLGA MWs, we observed that it is the polymer with higher MW that tends to have a stronger contribution to the final NP size. Prior work has shown that homogeneous NPs are obtained when the mixing time scale is smaller than that of the polymer aggregation time scale (typically in the several millisecond range).[32,33] Our studies reported here and previously[15] revealed that while small MW weight polymers (<30 kDa) were not very sensitive to mixing time, nanoprecipitation of high MW (>50 kDa) polymers exhibited distinct improvement in polydispersity upon rapid mixing. Nanoprecipitation involves nucleation of NPs and aggregation of polymers into NPs, resulting in the final size and polydispersity.[34] Rapid mixing results in rapid solvent exchange, and, therefore, the rate of nucleation is expected to be enhanced due to the higher supersaturation, directly contributing to a decrease in size. In addition, the barrier to insertion and aggregation depends on the solvent quality. Rapid transition to an aqueous solution is expected to increase the barrier required for insertion of polymers into NPs and the aggregation of NPs, due to the formation of a hydrophilic PEG layer on the surface. In the absence of complete solvent change, the PEG barrier may be insufficient to prevent aggregation, resulting in "tails" of larger NPs in the size distribution formed by aggregation of NPs. Our results suggest that this effect is prominent when the PLGA MW is high, which involves a larger driving force for aggregation due to the high MW hydrophobic block and a less effective barrier to aggregation due to the relatively low fraction of PEG. As a result, NPs prepared from high MW polymers tend to exhibit a greater sensitivity to mixing time. Although models have been developed to describe this process,[34] full details of the evolution of the barrier strength remain elusive.

We evaluated the NPs *in vitro* for macrophage uptake, which had two purposes: (a) to investigate the correlation between phagocytosis *in vitro* and blood clearance *in vivo* with the aim of rapid identification of NPs that would have lower probability of being successful *in vivo* (which saves significant time and resources); (b) to demonstrate the broad applicability of the platform by integrating it with a conventional NP assay; this can potentially be extended to high-throughput assays for other key NP biological properties such as complement activation, cell uptake, and cell cytotoxicity. The results indicate that NPs with significantly distinct macrophage uptake would likely have distinct pharmacokinetic profiles (though NPs with similar macrophage uptake would not necessarily exhibit similar pharmacokinetics). In addition, while it is known that NP size, PEG MW, and PEG wt % on NPs are factors that affect macrophage uptake, the results indicate that, over the range studied, NP size was a greater contributor to macrophage uptake than PEG MW and PEG wt % (*i.e.*, a smaller NP with shorter PEG would be taken up less than a larger NP with longer PEG). Consequently, our method to reproducibly synthesize NPs together with the *in vitro* macrophage uptake assay might be useful to quickly select promising NP formulations for preclinical evaluation with respect to circulation time, as well as to identify which formulations have a high probability of not working *in vivo*, which can save a significant amount of time and resources later on.

Integration of the microfluidic system with conventional high-throughput screening methods demonstrates versatility of the platform as well as broad applicability. The simple design of the device, the use of "off the shelf" materials such as PDMS, syringe pumps, 96-well plates, *etc.*, and the integration with high-throughput flow cytometry and screening in multiwell plates make it a technology and an approach relatively easy to replicate and adopt by other laboratories. Some limitations of the device are the time (∼hours) required to produce NPs at a scale larger than a few milligrams. To solve this challenge, one can parallelize the channels[35,36] or use mixers that have inherently high flow rates.[6,32] Similarly, the PDMS device tends to become less robust at high flow rates due to the high pressure exerted. This problem may be addressed by fabricating devices from stronger materials such as glass.

In this study we have identified the optimal ligand density that would result in minimal NP recognition by macrophages (which positively impacts the circulation time of NPs) and maximal uptake by LNCaP cells (which positively impacts the tumor accumulation of NPs). Assuming a NP density of 1.27 g/mL, the corresponding ligand density for the optimal NP is estimated at ~200 ligands/NP assuming that all ligands are expressed on the NP surface.[21] Since "optimal" is defined in the context of a desired effect, we expect that the optimal ligand density would vary with the choice of ligand, tumor/organ being targeted, and the cell type within the tumor/organ.

The use of a small-molecule, hydrophilic, and neutral targeting ligand, together with the ability to control the number of ligands on the surface of NPs, and the rapid mixing environment during self-assembly enable the one-step self-assembly of targeted NPs with similar size and charge to nontargeted NPs. While previous studies have investigated the impact of targeting on NP tumor accumulation,[26,37] any conclusive outcome is compromised by the differences in other properties of NPs (*e.g.*, increase in size) when a targeting ligand is added. Microfluidics enables synthesis of homogeneous NPs, and the impact of adding a longer MW polymer precursor on NP size is minimal compared to conventional synthesis, where NP size is significantly altered.[33] We can thus directly assess the impact of targeting, as the TNPs and NT-NPs in this study had the same size and zeta potential. These results, therefore, indicate that the incorporation of a targeting ligand on the surface of NPs does have a significant impact in the accumulation of NPs in the tumor when compared to nontargeted NPs with similar biophysicochemical properties (*e.g.*, size and zeta potential). While further studies should be carried out to investigate the kinetics of tumor accumulation, these preliminary results illustrate the importance of active targeting for tumor accumulation, and demonstrate the benefit of the microfluidic platform to rapidly identify a promising targeted NP candidate.

CONCLUSION

We reported a new microfluidic platform for the rapid, combinatorial synthesis of targeted polymeric NPs. It was first demonstrated that NPs with a wide range of properties can be generated by making a small library composed of NPs with sizes from 25 to 200 nm, zeta potentials from −20 to +20 mV, ligand densities from 0 to ~10^5 ligands/μm^2, and drug loadings from 0 to 5%. Subsequently, we showed the rapid NP development capabilities of the system by synthesizing 45 NP formulations of different sizes and PEG coverage and screened them against macrophage uptake *in vitro*. Finally we investigated the relation between *in vitro* macrophage uptake and *in vivo* pharmacokinetics, where low macrophage uptake correlated with longer circulation time. Building upon the *in vitro* macrophage uptake screen, we synthesized and screened targeted NPs to identify a formulation that maximized specific uptake *in vitro* while minimizing macrophage uptake. We also investigated the tumor accumulation of TNPs *versus* NT-NPs of essentially identical biophysicochemical properties, where the TNPs showed 3.5-fold accumulation in tumor *versus* nontargeted ones. Three key advantages of our system over existing bulk synthesis include the following: (i) from a small set of NP precursors one can rapidly synthesize a NP library with a wide range of distinct physicochemical properties; (ii) the NPs prepared have high batch-to-batch reproducibility; (iii) NPs can be prepared at different scales (*e.g.*, microgram *versus* milligram) without varying substantially the NP properties. These advantages allow for both *in vitro* and *in vivo* screening with the goals of either accelerating the clinical translation of a specific formulation or obtaining a deeper fundamental understanding on the correlation of NP properties and biological behavior.

MATERIALS AND METHODS

Materials. PLGA-PEG with PLGA MWs of 27, 45, and 95 kDa were purchased from Boehringer Ingelheim GmbH (Germany). PLGA-PEG with a PLGA MW of 10k Da was purchased from Akina Inc. (West Lafayette, IN, USA). Unmodified PLGA with MWs of 15k, 45k, and 70k were purchased from Lactel (Pelham, AL, USA). All PEG-based polymers were purchased from Laysan Bio, Inc. (Arab, AL, USA). Alexa Fluor probes as well as all biological reagents were purchased from Invitrogen (Carlsbad, CA, USA). Cell lines were purchased from ATCC (Manassas, VA, USA). Balb/c mice were purchased from Charles River Laboratories (Wilmington, MA, USA). All solvents were purchased from Sigma-Aldrich (St. Louis, MO, USA). Docetaxel was purchased from LC Laboratories (Woburn, MA, USA). Finally, SU-8 and PDMS were purchased from Microchem (Newton, MA, USA) and Dow Corning (Midland, MI, USA).

Fabrication of Microfluidic System. The prototypical system was manufactured using standard soft lithography, described previously.[33] Briefly, SU-8 resist was lithographically patterned on a 4 in. silicon wafer to fabricate a master mold. Polydimethylsiloxane (Sylgard 184) monomer and curing agent were mixed in a ratio of 10:1 by weight, poured over the silicon master mold, and degassed. After curing at 100 °C for 60 min, the PDMS cast was carefully removed from the mold. The multi-inlet mixing unit was composed of two layers that were aligned and bonded together after placing each layer in plasma for 30 s. Inlets and outlet holes were drilled followed by bonding the PDMS to a glass slide using air plasma. The NP synthesis unit was composed of a single layer with inlet holes precisely drilled next to each other to achieve 3D flow focusing.[15] Typical channel dimensions used in the NP synthesis experiments had a width of 100 μm and a height of 60 μm for the vertical focusing part and had a width of 20 μm for the horizontal focusing part, or precipitation channel. The outlet of the mixer unit was connected to the middle inlet in the NP synthesis unit, while the side inlets were connected to syringes containing acetonitrile.

Nanoparticle Precursors. PLGA-PEG-LIG was synthesized as previously reported.[18] Briefly, LIG was dissolved in 400 μL of dimethylformamide (DMF) and allowed to react with tBOC-NH-PEG-NHS in the presence of *N*,*N*-diisopropylethylamine (DIEA). The reaction product was dialyzed for 24 h in water to remove unreacted LIG, then lyophilized, and finally resuspended in trifluoroacetic acid to remove tBOC. Subsequently, PEG-LIG was dried and dissolved in DMSO. In parallel, PLGA-COOH was allowed to react with *N*-hydroxysuccinimide (NHS) in the presence of 1-ethyl-3-[3-dimethylaminopropyl] carbodiimide (EDC) in dichloromethane (DCM). The resulting PLGA-NHS was dried and dissolved in DMSO. Finally, PEG-LIG and PLGA-NHS in DMSO were mixed with DIEA, allowed to react, precipitated in cold methanol, and dried under vacuum.

Synthesis of PLGA-PEG was accomplished using EDC/NHS chemistry.[22] Synthesis of PLGA-PEG with PEG of different PEG MWs and PEG functional groups was accomplished by conjugation of PLGA homopolymer with a carboxylate end-group to a monofunctional methoxy-PEG$_x$-NH$_2$, where *x* indicates PEG MW (2, 5, and 10 kDa). For PLGA-PEG functionalized with carboxyl and amine groups, difunctional NH$_2$-PEG-COOH and NH$_2$-PEG-NH$_2$ were used, respectively. Briefly, PLGA-carboxylate was dissolved in DCM, followed by the addition of NHS and EDC to the solution. After 2 h the resulting product, PLGA-NHS, was precipitated in ethyl ether/methanol, collected by centrifugation, and dried under vacuum. PLGA-NHS was dissolved in DCM followed by addition of monofunctional or difunctional PEG together with DIEA. The resulting PLGA-PEG block copolymer was precipitated with ether/methanol and washed with the same solvent to remove unreacted PEG.

The syntheses of PLGA-Alexa488 and PLGA-Alexa647 were accomplished by the conjugation of an activated PLGA-COOH with Alexa Fluor-488/647 Cadaverine through EDC/NHS conjugation. First, Alexa Fluor-488/647 was dissolved in 1 mL of DMF. Concurrently, PLGA-COOH was mixed with EDC and NHS in 500 μL of DMF. Finally, PLGA solution was reacted with Alexa Fluor-488/647 solution for 16 h at room temperature. The reaction product was precipitated in ice cold methanol and dried under vacuum. All polymers were characterized with gel permeation chromatography as well as nuclear magnetic resonance, to confirm molecular weight and chemical structure, respectively.

Nanoparticle Synthesis and Characterization. NPs were prepared by nanoprecipitation.[15] Briefly, the organic stream (polymers and drugs) was run at 7 μL/min, and vertical sheath streams (acetonitrile) were run at 3 μL/min while maintaining a total aqueous flow rate of 50 μL/min. NPs were collected at the outlet stream and washed three times with water using an Amicon centrifugation filtration membrane to remove excess drugs and organic solvents. Dynamic light scattering was used to determine particle size and size distribution, using a Zetasizer Nano ZS instrument (Malvern Instruments Ltd., U.K.). Particle visualization was carried out through TEM (JEOL 2011 instrument at an acceleration voltage of 200 kV). Drug loading and encapsulation efficiency were determined by quantifying the amount of docetaxel in the NP by dissolving them in a 50/50 acetonitrile/water solution immediately after synthesis and vortexing for several hours to induce NP dissociation. The amount of docetaxel inside the NPs was quantitated by HPLC with a UV reader at a wavelength of 267 nm. A calibration curve with known concentrations of docetaxel was prepared, and the amount of drug encapsulated in the NPs was calculated accordingly.

Nanoparticle Binding and Uptake by RAW264.7 and LNCaP Cells. RAW 264.7 cells were cultured in DMEM medium with 10% fetal bovine serum, 50 units/mL penicillin, and 50 mg/mL streptomycin. LNCaP cells were cultured in RPMI medium with 10% fetal bovine serum, 50 units/mL penicillin, and 50 mg/mL streptomycin. Cells were seeded at a density of 50 000 cells per well on a 24-well plate. After 24 h, the cell medium was removed and replaced with NPs dissolved in the same medium at a concentration of 1 mg/mL. Cells and NPs were incubated for 4 h for the case of RAW 264.7 and LNCaP, followed by three washes with 1% BSA solution in PBS to remove excess NPs. RAW264.7 cells were removed from the plate using a cell scraper and centrifuged, while LNCaP cells were treated with trypsin, removed from the plate, and centrifuged. The resultant cell pellets were reconstituted in 250 μL of PBS and placed on a 96-well plate for FACS analysis. Flow cytometry analysis was performed on a BD Biosciences LSR II with high-throughput sampler (HTS) option, with 10 000 cells collected for each measurement.

Pharmacokinetics and Biodistribution Studies. All animal studies were conducted under the supervision of MIT's Division of Comparative Medicine in compliance with the NIH's Principles of Laboratory Animal Care. For pharmacokinetic studies, wild-type Balb/c mice were used. Fluorescently labeled NPs (with Alexa-647) were injected *via* tail vein in groups of four mice per formulation. At different time points, a few microliters of blood was sampled from the mouse, and the fluorescence measured using an IVIS imaging system. As a control, blood from mice with no NPs injected was used and the background fluorescence was measured. Plasma half-life was determined using the method described by H. Cabral *et al.*,[38] whereas area under the curve was calculated by integrating the PK profile using the trapezoid method.

For biodistribution studies, the xenograft tumor-bearing mouse model was constructed by inoculating 1×10^7 cells/0.2 mL mixed with an equal volume of ice-cold matrigel. The cells employed were luciferase-expressing LNCaP cells (LNCap-luc), which allow for continuously monitoring and controlling the growth of the tumor by whole-animal luminescent imaging. Tumors were allowed to grow for 3−4 weeks until they reached a relative luminescence intensity of $\sim(1.5-2.5) \times 10^6$ photons/s, which corresponds to tumor sizes of 400−600 mm^3. Mice were randomized into targeted NPs and nontargeted NPs treatment groups (n = 5 each). To each mouse was injected 200 μL of a solution containing 5 mg/mL of NPs labeled with Alexa-647 *via* tail vein. The fluorescence of each formulation did not vary significantly between each dose or between NT-NP and TNP. After 24 h the animals were sacrificed, main organs were excised and weighed, and their fluorescence was measured using an IVIS spectrum-bioluminescent and fluorescent imaging system (Xenogen Corporation).

Conflict of Interest: The authors declare the following competing financial interest(s): O.C.F. and R.L. disclose financial interest in BIND Biosciences, Selecta Biosciences, and Blend Therapeutics, biotechnology companies developing nanoparticle technologies for medical applications. These companies did not support the aforementioned work and currently have no rights to any technology or intellectual property developed as part of this work.

Acknowledgment. This work was supported by the Koch-Prostate Cancer Foundation Award in Nanotherapeutics (R.L. and O.C.F.), the National Cancer Institute (NCI) Center of Cancer Nanotechnology Excellence at MIT-Harvard (U54-CA151884, R.L. and O.C.F.), and the National Heart, Lung, and Blood Institute (NHLBI) Programs of Excellence in Nanotechnology (HHSN268201000045C; R.L. and O.C.F.). P.M.V. is supported by the National Science Foundation (NSF) graduate research fellowship. E.M.P. is supported by an NDSEG graduate research fellowship and a Center of Cancer Nanotechnology Excellence graduate research fellowship (5 U54 CA151884-02).

Supporting Information Available: Additional details on (1) NP precursors used for the synthesis of NP library with a wide range of physicochemical properties; (2) polymer precursors, NP size, PEG wt %, and average PEG MW of NPs synthesized and screened against macrophages; (3) batch-to-batch reproducibility of targeted NPs prepared in the microfluidic system and comparison of size distribution obtained by microfluidic synthesis *versus* bulk synthesis; and (4) average size and zeta potential of nontargeted NPs and targeted NPs. This material is available free of charge *via* the Internet at http://pubs.acs.org.

REFERENCES AND NOTES

1. Peer, D.; Karp, J. M.; Hong, S.; Farokhzad, O. C.; Margalit, R.; Langer, R. Nanocarriers as an Emerging Platform for Cancer Therapy. *Nat. Nanotechnol.* **2007**, *2*, 751–760.

2. Shi, J.; Xiao, Z.; Kamaly, N.; Farokhzad, O. C. Self-Assembled Targeted Nanoparticles: Evolution of Technologies and Bench to Bedside Translation. *Acc. Chem. Res.* **2011**, *44*, 1123–1134.
3. Hrkach, J.; Von Hoff, D.; Ali, M.; Andrianova, E.; Auer, J.; Campbell, T.; de Witt, D.; Figa, M.; Figueiredo, M.; Horhota, A.; *et al*. Preclinical Development and Clinical Translation of a PSMA-Targeted Docetaxel Nanoparticle with a Differentiated Pharmacological Profile. *Sci. Transl. Med.* **2012**, *4*, 1–11.
4. Murday, J. S.; Siegel, R. W.; Stein, J.; Wright, J. F. Translational Nanomedicine: Status Assessment and Opportunities. *Nanomedicine* **2009**, *5*, 251–273.
5. Chan, E. M.; Xu, C.; Mao, A. W.; Han, G.; Owen, J. S.; Cohen, B. E.; Milliron, D. J. Reproducible, High-Throughput Synthesis of Colloidal Nanocrystals for Optimization in Multidimensional Parameter Space. *Nano Lett.* **2010**, *10*, 1874–1885.
6. Kim, Y.; Lee Chung, B.; Ma, M.; Mulder, W. J.; Fayad, Z. A.; Farokhzad, O. C.; Langer, R. Mass Production and Size Control of Lipid-Polymer Hybrid Nanoparticles through Controlled Microvortices. *Nano Lett.* **2012**, *12*, 3587–3591.
7. Wang, H.; Liu, K.; Chen, K. J.; Lu, Y.; Wang, S.; Lin, W. Y.; Guo, F.; Kamei, K.; Chen, Y. C.; Ohashi, M.; *et al*. A Rapid Pathway toward a Superb Gene Delivery System: Programming Structural and Functional Diversity into a Supramolecular Nanoparticle Library. *ACS Nano* **2010**, *4*, 6235–6243.
8. Whitesides, G. M. The Origins and the Future of Microfluidics. *Nature* **2006**, *442*, 368–373.
9. Jahn, A.; Reiner, J. E.; Vreeland, W. N.; DeVoe, D. L.; Locascio, L. E.; Gaitan, M. Preparation of Nanoparticles by Continuous-Flow Microfluidics. *J. Nanopart. Res.* **2008**, *10*, 925–934.
10. Chen, D.; Love, K. T.; Chen, Y.; Eltoukhy, A. A.; Kastrup, C. J.; Sahay, G.; Jeon, A.; Dong, Y.; Whitehead, K. A.; Anderson, D. G. Rapid Discovery of Potent siRNA-Lipid-Nanoparticles Enabled by Controlled Microfluidic Formulation. *J. Am. Chem. Soc.* **2012**, *134*, 6948–6951.
11. Valencia, P. M.; Farokhzad, O. C.; Karnik, R.; Langer, R. Microfluidic Technologies for Accelerating the Clinical Translation of Nanoparticles. *Nat. Nanotechnol.* **2012**, *7*, 623–629.
12. Dolle, R. E. Historical Overview of Chemical Library Design. *Methods Mol. Biol.* **2011**, *685*, 3–25.
13. Macarron, R.; Banks, M. N.; Bojanic, D.; Burns, D. J.; Cirovic, D. A.; Garyantes, T.; Green, D. V.; Hertzberg, R. P.; Janzen, W. P.; Paslay, J. W.; *et al*. Impact of High-Throughput Screening in Biomedical Research. *Nat. Rev. Drug Discovery* **2011**, *10*, 188–195.
14. Siegwart, D. J.; Whitehead, K. A.; Nuhn, L.; Sahay, G.; Cheng, H.; Jiang, S.; Ma, M.; Lytton-Jean, A.; Vegas, A.; Fenton, P.; *et al*. Combinatorial Synthesis of Chemically Diverse Core-Shell Nanoparticles for Intracellular Delivery. *Proc. Natl. Acad. Sci. U.S.A.* **2011**, *108*, 12996–13001.
15. Rhee, M.; Valencia, P. M.; Rodriguez, M. I.; Langer, R.; Farokhzad, O. C.; Karnik, R. Synthesis of Size-Tunable Polymeric Nanoparticles Enabled by 3D Hydrodynamic Flow Focusing in Single-Layer Microchannels. *Adv. Mater.* **2011**, *23*, H79–83.
16. Xia, H. M.; Wan, S. Y.; Shu, C.; Chew, Y. T. Chaotic Micromixers Using Two-Layer Crossing Channels to Exhibit Fast Mixing at Low Reynolds Numbers. *Lab Chip* **2005**, *5*, 748–755.
17. Chandran, S. S.; Banerjee, S. R.; Mease, R. C.; Pomper, M. G.; Denmeade, S. R. Characterization of a Targeted Nanoparticle Functionalized with a Urea-Based Inhibitor of Prostate-Specific Membrane Antigen (PSMA). *Cancer Biol. Ther.* **2008**, *7*, 974–982.
18. Valencia, P. M.; Pridgen, E. M.; Perea, B.; Gadde, S.; Sweeney, C.; Kantoff, P. W.; Bander, N. H.; Lippard, S. J.; Langer, R.; Karnik, R.; *et al*. Synergistic Cytotoxicity of Irinotecan and Cisplatin in Dual-Drug Targeted Polymeric Nanoparticles. *Nanomedicine (London, U.K.)* **2012**, *8*, 687–698.
19. Valencia, P. M.; Basto, P. A.; Zhang, L.; Rhee, M.; Langer, R.; Farokhzad, O. C.; Karnik, R. Single-Step Assembly of Homogenous Lipid-Polymeric and Lipid-Quantum Dot Nanoparticles Enabled by Microfluidic Rapid Mixing. *ACS Nano* **2010**, *4*, 1671–1679.
20. Salvador-Morales, C.; Zhang, L.; Langer, R.; Farokhzad, O. C. Immunocompatibility Properties of Lipid-Polymer Hybrid Nanoparticles with Heterogeneous Surface Functional Groups. *Biomaterials* **2009**, *30*, 2231–2240.
21. Valencia, P. M.; Hanewich-Hollatz, M. H.; Gao, W.; Karim, F.; Langer, R.; Karnik, R.; Farokhzad, O. C. Effects of Ligands with Different Water Solubilities on Self-Assembly and Properties of Targeted Nanoparticles. *Biomaterials* **2011**, *32*, 6226–6233.
22. Cheng, J.; Teply, B. A.; Sherifi, I.; Sung, J.; Luther, G.; Gu, F. X.; Levy-Nissenbaum, E.; Radovic-Moreno, A. F.; Langer, R.; Farokhzad, O. C. Formulation of Functionalized PLGA-PEG Nanoparticles for *in Vivo* Targeted Drug Delivery. *Biomaterials* **2007**, *28*, 869–876.
23. Avgoustakis, K. Pegylated Poly(Lactide) and Poly(Lactide-Co-Glycolide) Nanoparticles: Preparation, Properties and Possible Applications in Drug Delivery. *Curr. Drug Delivery* **2004**, *1*, 321–333.
24. Gref, R.; Luck, M.; Quellec, P.; Marchand, M.; Dellacherie, E.; Harnisch, S.; Blunk, T.; Muller, R. H. 'Stealth' Corona-Core Nanoparticles Surface Modified by Polyethylene Glycol (PEG): Influences of the Corona (PEG Chain Length and Surface Density) and of the Core Composition on Phagocytic Uptake and Plasma Protein Adsorption. *Colloids Surf., B* **2000**, *18*, 301–313.
25. Perrault, S. D.; Walkey, C.; Jennings, T.; Fischer, H. C.; Chan, W. C. Mediating Tumor Targeting Efficiency of Nanoparticles through Design. *Nano Lett.* **2009**, *9*, 1909–1915.
26. Kamaly, N.; Xiao, Z.; Valencia, P. M.; Radovic-Moreno, A. F.; Farokhzad, O. C. Targeted Polymeric Therapeutic Nanoparticles: Design, Development and Clinical Translation. *Chem. Soc. Rev.* **2012**, *41*, 2971–3010.
27. Ma, L. L.; Jie, P.; Venkatraman, S. S. Block Copolymer 'Stealth' Nanoparticles for Chemotherapy: Interactions with Blood Cells *in Vitro*. *Adv. Funct. Mater.* **2008**, *18*, 716–725.
28. Bertrand, N.; Leroux, J. C. The Journey of a Drug-Carrier in the Body: An Anatomo-Physiological Perspective. *J. Controlled Release* **2011**, *161*, 152–163.
29. Shan, X.; Liu, C.; Yuan, Y.; Xu, F.; Tao, X.; Sheng, Y.; Zhou, H. *In Vitro* Macrophage Uptake and *in Vivo* Biodistribution of Long-Circulation Nanoparticles with Poly(Ethylene-Glycol)-Modified PLA (BAB Type) Triblock Copolymer. *Colloids Surf., B* **2009**, *72*, 303–311.
30. Sheng, Y.; Yuan, Y.; Liu, C.; Tao, X.; Shan, X.; Xu, F. *In Vitro* Macrophage Uptake and *in Vivo* Biodistribution of PLA-PEG Nanoparticles Loaded with Hemoglobin as Blood Substitutes: Effect of PEG Content. *J. Mater. Sci. Mater. Med.* **2009**, *20*, 1881–1891.
31. Perry, J. L.; Reuter, K. G.; Kai, M. P.; Herlihy, K. P.; Jones, S. W.; Luft, J. C.; Napier, M.; Bear, J. E.; Desimone, J. M. PEGylated PRINT Nanoparticles: The Impact of PEG Density on Protein Binding, Macrophage Association, Biodistribution, and Pharmacokinetics. *Nano Lett.* **2012**, *12*, 5304–5310.
32. Johnson, B. K.; Prud'homme, R. K. Mechanism for Rapid Self-Assembly of Block Copolymer Nanoparticles. *Phys. Rev. Lett.* **2003**, *91*, 118302–118305.
33. Karnik, R.; Gu, F.; Basto, P.; Cannizzaro, C.; Dean, L.; Kyei-Manu, W.; Langer, R.; Farokhzad, O. C. Microfluidic Platform for Controlled Synthesis of Polymeric Nanoparticles. *Nano Lett.* **2008**, *8*, 2906–2912.
34. Lince, F.; Marchisio, D. L.; Barresi, A. A. Strategies to Control the Particle Size Distribution of Poly-Epsilon-Caprolactone Nanoparticles for Pharmaceutical Applications. *J. Colloid Interface Sci.* **2008**, *322*, 505–515.
35. Kang, X.; Luo, C.; Wei, Q.; Xiong, C.; Chen, Q.; Chen, Y.; Ouyang, Q. Mass Production of Highly Monodisperse Polymeric Nanoparticles by Parallel Flow Focusing System. *Microfluid Nanofluid* **2013**, *15*, 337–345.
36. Lim, J. M.; Bertrand, N.; Valencia, P. M.; Rhee, M.; Langer, R.; Jon, S.; Farokhzad, O. C.; Karnik, R. Parallel Microfluidic Synthesis of Size-Tunable Polymeric Nanoparticles Using

3D Flow Focusing toward *in Vivo* Study. *Nanomedicine* **2013**, in press.
37. Huynh, N. T.; Roger, E.; Lautram, N.; Benoit, J. P.; Passirani, C. The Rise and Rise of Stealth Nanocarriers for Cancer Therapy: Passive *versus* Active Targeting. *Nanomedicine (London, U.K.)* **2010**, *5*, 1415–1433.
38. Cabral, H.; Matsumoto, Y.; Mizuno, K.; Chen, Q.; Murakami, M.; Kimura, M.; Terada, Y.; Kano, M. R.; Miyazono, K.; Uesaka, M.; *et al*. Accumulation of Sub-100 nm Polymeric Micelles in Poorly Permeable Tumours Depends on Size. *Nat. Nanotechnol.* **2011**, *6*, 815–823.